Supplementary Materials for

Fructose-driven glycolysis supports anoxia resistance in the naked mole-rat

Thomas J. Park,*† Jane Reznick,† Bethany L. Peterson, Gregory Blass, Damir Omerbašić, Nigel C. Bennett, P. Henning J. L. Kuich, Christin Zasada, Brigitte M. Browe, Wiebke Hamann, Daniel T. Applegate, Michael H. Radke, Tetiana Kosten, Heike Lutermann, Victoria Gavaghan, Ole Eigenbrod, Valérie Bégay, Vince G. Amoroso, Vidya Govind, Richard D. Minshall, Ewan St. J. Smith, John Larson, Michael Gotthardt, Stefan Kempa, Gary R. Lewin*

*Corresponding author. Email: glewin@mdc-berlin.de (G.R.L.); tpark@uic.edu (T.J.P.)

†These authors contributed equally to this work.

Published 21 April 2017, *Science* **356**, 307 (2017)
DOI: 10.1126/science.aab3896

This PDF file includes:

Other Supplementary Material for this manuscript includes the following:
(available at www.sciencemag.org/content/356/6335/307/suppl/DC1)

Materials and Methods

In vivo experiments

All animal protocols were approved by the University of Illinois at Chicago Institutional Animal Care and Use Committee, the German federal authorities (State of Berlin), or the animal use and care committee of the University of Pretoria, Republic of South Africa.

Animals were placed into a clear plastic chamber pre-filled with the desired gas mixture. Thereafter the chamber was infused continuously at 10 liters per minute. Using an Ocean Optics Foxy-PI200 probe, and an Ocean Optics sensor connected to a computer, we measured the fill time, which was, on average, 59.7 ± 2.3 seconds (standard error). Based on the data, we pre-filled the chamber for 120 seconds prior to introducing the animal. Each animal was video recorded for the collection of accurate timing data.

ECGs were recorded non-invasively using the ECGenie recording enclosure (Mouse Specifics, Inc., Boston, MA, USA) (*30*). In brief, the ECGenie system comprises a platform with embedded paw-sized AgCl ECG electrodes connected to an amplifier (e-MOUSE). Signals were collected and analysed using PowerLab and LabChart (ADInstruments, version 7). A peak detection algorithm on LabChart enabled R-wave identification using Fourier analysis and linear time-invariant digital filtering of frequencies below 3 Hz and above 100 Hz to minimize environmental signal disturbances. Only data from continuous recordings were used in the analyses. The signals were digitized at a sampling rate of 2 kHz. Baseline heart data were acquired on conscious animals after which animals were placed in an N_2 filled chamber with a continuous stream of N_2 gas. Shortly after N_2 exposure the animal became unconscious and ECG was recorded by placing each of the front paws of the unconscious animal on a

single electrode. Breaths were recorded visually and counted by an observer with a manual counter.

Naked mole-rats were kept on a heated mat to maintain their body temperature at 30° or 37°. Body temperature was measured with a digital rectal probe (Fine Science Tools TR-100).

Pulmonary edema measurements were made as follows. Animals were exposed to a desired gas mixture for 15 minutes. Following exposure, the animal was immediately decapitated and the lungs removed and weighed. The lungs were then dried overnight and weighed again to generate a wet-to-dry weight ratio which was used as an assay of lung edema.

Isolated heart

Perfusion and ischemia induction in isolated heart preparations: 12 week old mice and 3 to 11 year old naked mole rats were sacrificed by cervical dislocation or decapitation, respectively. Hearts were quickly removed and immersed in ice-cold modified Krebs-Henseleit (KH) solution, containing: 111.8 mM NaCl; 24.7 mM NaHCO3; 4.7 mM KCl; 2.1 mM MgSO4; 1.2 mM KH2PO4; 2.0 mM CaCl2; 0.06 mM EDTA; 11.1 mM glucose. The aorta was immediately cannulated for retrograde perfusion with KH solution at a constant pressure of 80 mmHg. The buffer solution was saturated with 95% O2 / 5 % CO2. To measure left ventricular developed pressure (LVDP), a balloon was placed into the left ventricle through the left articular appendage and inflated to maintain a constant end diastolic pressure of 5-10 mmHg. Measurements were performed at 30 °C or 37 °C as indicated. After an adjustment time of 30 min cardiac activity was stable (baseline)

and a global ischemia was induced by stopping the coronary flow for 30 min. The flow was set back to normal during the re-perfusion phase for 30 min. Recovery of cardiac function was calculated as left ventricular developed pressure (LVDP) post ischemia compared to baseline values. For fructose treatment, a second KH solution was substituted with 11.1 mM fructose instead of glucose and treated as described above with a 30 minute adjustment phase before switching to fructose buffer for 60 min. The flow was set back to glucose for 30 min and the last two steps were repeated. Heart rate, systolic pressure, and diastolic pressure were recorded throughout the entire measurement.

Metabolites

At each time point, animal tissues were removed and snap-frozen in liquid nitrogen. All tissues were powdered while frozen using a BioPulverizer (BioSpec Products, Cat. No. 59012N). Powdered samples were resolved in ice-cold MCW (methanol:chloroform:water, 5:2:1), vortexed, and shaken for 45 minutes at 4°C. MilliQ water was then added (1/2 of initial MCW volume) to induce phase separation, vortexed, and shaken for 15 minutes at 4°C. Samples were centrifuged in a table top centrifuge at 20,000 g for 10 minutes. The resulting polar and apolar phases were collected and subsequently dried in a rotational vacuum concentrator (Martin Christ, Speed Vac RVC 2-33 CD, Cooling Trap alpha 2-4 LD plus) and then frozen at -20 °C until derivatization.

Brain Slice labelling/harvest

Mice and naked mole-rats were decapitated and the brains were rapidly removed into ice-cold artificial cerebrospinal fluid (ACSF) containing (in mM): NaCl, 124; KCl, 3; KH2PO4, 1.2; NaHCO3, 26; MgSO4, 2.5; CaCl2, 3.4; Na-ascorbate, 2; and D-glucose,

10, gassed with 95% O2 and 5% CO2. The tissue was then sliced at 400 mm with a vibrotome. Slices were briefly washed in ACSF buffer containing no glucose. For labeling experiments 10mM glucose in the ACSF buffer was replaced with 10mM ^{13}C6-Fructose (Sigma-Aldrich). Slices were incubated for 0, 5, 15 and 30 mins at 32 degrees after which the brains were washed 2 times in label-free buffer (140 mM NaCl, 5 mM HEPES, pH7.4) and snap frozen. Frozen brain slices were powdered and 50mg of tissue was used for extraction. The experiments were performed on three animals per species.

Metabolomics sample preparation

Metabolite extraction, derivatization, GC-MS analysis and measurement was performed as described with slight modifications (*14*). One milliliter ice-cold Methanol-chloroform-water MCW (5:2:1) containing 2µg/ml cinnamic acid was added to 50mg of powdered tissue and shaken for 30 min at 4°C to separate lipid and polar intermediates, after which 500uL of water was added to each sample, shaken for further 10 min and centrifuged at maximum speed for 10 min for phase separation. Polar phase was collected and dried under a vacuum.

Derivatization was carried out by dissolving dry tissue extracts in 20 µl of methoxyamine hydrochloride solution (Sigma, 40 mg/ml in pyridine (Roth)) and incubated for 90 min at 30°C with constant shaking followed by the addition of 80 µl of N-methyl-N-[trimethylsilyl]trifluoroacetamide (MSTFA; Machery-Nagel, Dueren, Germany) and incubation at 37°C for 45 min. The extracts were centrifuged for 10 min at 10,000 × g, and aliquots of 30 µl were transferred into glass vials (Th. Geyer, Berlin, Germany) for gas chromatography-mass spectrometry (GC-MS) measurement.

Retention index standards and quantification standards

Nine alkanes (n-decane, n-dodecane, n-pentadecane, n-octadecane, n-nonadecane, n-docosane, n-octacosane, n-dotriacontane, and n-hexatriacontane) were dissolved in hexane, combined at a final concentration of 2 mg/ml and stored at 4°C. Retention index standard was added to the solvent (MSTFA) at a final concentration of 2% (v/v) during derivatization.

The quantification mixture was composed of 63 compounds (stock concentration 1 mg/ml, 20% MeOH). A dilution series from 1:1, 1:2, 1:5, 1:10, 1:20, 1:50, 1:100, and 1:200 was prepared (*14*), portioned, dried under vacuum, and stored at -20°C. One set of quantification standards was prepared for GC-MS measurements and measured in technical replicates within the experiment (standards were available for 63/80 metabolites measured, including all key metabolites described in the results).

GC-MS measurement

Metabolite analysis was performed on a gas chromatography coupled to time of flight mass spectrometer (Pegasus III- TOF-MS-System, LECO Corp., St. Joseph, MI, USA), complemented with an auto-sampler (MultiPurpose Sampler 2 XL, Gerstel, Mülheim an der Ruhr, Germany). The samples and quantification standards were injected in splitless and split mode (split 1:5, injection volume 1 µl) in a temperature-controlled injector (CAS4, Gerstel) with a baffled glass liner (Gerstel). The following temperature program was applied during sample injection: initial temperature of 80°C for 30 s followed by a ramp with 12°C/min to 120°C and a second ramp with 7°C/min to 300°C and final hold for 2 min. Gas chromatographic separation was performed on an Agilent 6890 N (Agilent, Santa Clara, CA, USA), equipped with a VF-5 ms column of 30-m length, 250-

µm inner diameter, and 0.25-µm film thickness (Varian, Palo Alto, CA, USA). Helium was used as carrier gas with a flow rate of 1.2 ml/min. Gas chromatography was performed with the following temperature gradient: 2-min heating at 70°C, first temperature gradient with 5°C/min up to 120°C and hold for 30 s; subsequently, a second temperature increase of 7°C/min up to 200°C and a third elevation of 12°C/min up to 320°C with a hold time of 2 min. The spectra were recorded in a mass range of 60 to 600 U with 20 spectra/s at a detector voltage of 1750 V.

Data analysis

Data analysis was performed using ChromaTOF Version 4.42 (LECO) and Maui-VIA software as described previously (*14*, *15*). Calibration curves were determined for each intermediate by linear regression analysis of known quantities and the detected total peak areas of the top 5 most intense ions m/z from the quantification standards. Ions dependent on carbon-13 introduced intensity shift were complemented with their corresponding matches for the absolute quantification. Metabolite pool sizes have been calculated by assuming metabolic state and summarizing all quantities of the time-course pSIRM (pulsed stable isotope metabolomics) experiment. Only peak areas within the linear range of the calibration curve have been taken into account for the absolute quantification.

In the initial GS-MS experiment higher concentrations of glucose e.g. like those found in blood, were not included in the calibration and measured intensities fell outside of the calibration curve. To allow a robust quantification of glucose we ran higher concentration standards in a second experiment to obtain an extended calibration curve for the quantification of glucose concentrations in liver and blood. The applied concentrations allowed to obtain the upper limits of quantification (both on chromatography and mass

detector) (fig S8); the extended calibration curve showed saturation beyond the linear response of the GC-MS system. We then calculated the Response factor to adjust the new calibration to the original experimental run on a similar machine with identical settings. Finally, the measured glucose concentration were the linear range of the GC-MS system and thus glucose levels were absolutely quantified from the measured blood and liver samples. We measured glucose concentration in samples of blood taken from mice and naked mole-rats using a glucometer and found similar values to those calculated from the GC-MS experiment under basal conditions (fig S8).

The in-house-developed pSIRM-wizard enabled the quantification of ^{13}C-label incorporation based on the exported data following the descriptions and equations previously described (*14*). The stable isotope incorporation was determined for a set of pre-defined metabolite-specific fragments. Mass isotopomer distributions (MID) for each fragment were calculated and exported by MAUI-Via. The measurement of non-labeled standards facilitated the correction for natural carbon abundance. Standard MIDs were automatically extracted from measurements matching the concentration range of the sample. The $^{13}C_6$-fructose incorporation in CCM intermediates has been calculated carbon-position resolved by the application of the targeted approach (*14*). Labeled quantities were determined for each time point by multiplying the ^{13}C-incorporation of each measurement with the absolute metabolite pool. Statistical analysis was performed using a two-way ANOVA followed by Bonferroni post-hoc tests.

Sequence alignment

The amino acid sequences of guinea pig (H0VRF2), mouse (Q9WV38), rat (P43427) and human (P22732) GLUT5 were downloaded from UniProt (*31*), while naked mole-rat

(NMR, XP_004863723.1) sequences were retrieved from the RefSeq database(*32*). Multiple alignment of the GLUT5 protein sequences was performed using the MUSCLE software package with default parameters (*33*).

Ketohexokinase splice variant assay

The *Khk* splicing assay was adapted from previously published protocols (*29*). RNA isolated from naked mole-rat and mouse liver tissue was reverse-transcribed then amplified using a forward primer (mouse; 5′-GAAGCAGATCCTGTGCGTG-3′ and nmr; 5′-GAAGCGGATTCTGTGCGTG-3′) that bound to shared *Khk A/C* exon 1 and a reverse primer (mouse; 5′-ATTGTGCTCCTCTATCCGC-3′ and nmr; 5′-GCGTATAGAACAGCACAAT-3′) that bound to shared *Khk A/C* exon 5 sequences. The 468-bp PCR products representing both *Khk-A* and *Khk-C* transcripts were then digested with HincII and run on a 1.5% agarose gel. The 468 bp represents the uncut *Khk-A*-specific amplicon and the two lower bands at 294 bp and 174 bp represent HincII-cleaved *Khk-C*-specific amplicon.

qPCR

Total RNA was isolated from tissues using TRIzol reagent (Life Technologies), according to the manufacturer's instructions. After DNase digest, 0.65 μg of total RNA was reverse transcribed with Supersript III reverse polymerase (Invitrogen) and analyzed using Universal Probe Library. Gene Expression Assays on the ABI 7900 system (Applied Biosystems). The following primers were used to quantify mouse *Glut5* F: 5'-AGAGCAACGATGGAGGAAAA-3' R: 5'-CCAGAGCAAGGACCAATGTC-3' and

nmr *Glut5* F: 5'-GTGCCCCAGCTCTTCATC-3' R:5'-GTTCCGAAAACCGAACAGC-3', designed using the ProbeFinder Software with sequences retrieved for mouse (ENSMUST00000030826) and naked mole-rat (XM_004863666.1). To analyse KHK isoforms the following primer pairs were designed for mouse *Khk-A* F: 5'-TGGACTTACGATATGTGGTCCTT-3' R: 5'-GCCTCGTTGATGATGACTGTAG-3' and *Khk-C* F: 5'-GCGTGGATGTGTCTCAGGTG-3' R: TGTTGACGATGCAGCAAGA (reference sequence XM_006503749.1 and NM_008439.4, respectively.) and nmr *Khk-A* F: 5'-TCCGTGGACCTACGCTACTT-3' R: 5'-CTCGCTGATGATGACTGTGG-3' and nmr *Khk-C* F: 5'-CGTGGATGTGTCTCAGGTGT-3' and R: 5'-AGATGTTGACGATGCAGCAG-3' (reference sequence XM_004839170.1 and XM_004839169.1, respectively). To calculate absolute numbers of transcripts, plasmids were made containing the cDNA amplicon from each primer pair for mouse and nmr. The standard curve method with known doses of plasmid was used to quantitate mRNA transcripts by extrapolating a value by comparing unknowns to the standard curve of known transcript amounts.

Immunoblotting

Tissues were lysed with RIPA buffer (50 mM Tris-HCL, pH 7.5, 150 mM NaCl, 1% Nonidet NP40, 0.5% sodium deoxycholate, 1% SDS) containing CHAPS (Sigma) and protein inhibitor cocktail (Roche) and protein concentration was determined using the Bradford reagent (BioRad). Thirty micrograms of proteins were separated by SDS-PAGE, followed by Western blot analysis using rabbit Glut5 (SLC2A5) antibody (PA5-42100, Thermofischer), mouse GAPDH antibody (6C5, Calbiochem) and mouse anti b actin (A1978, Sigma). Appropriate horseradish peroxidase-conjugated secondary

antibodies were used for chemiluminescence (ECL, Millipore or Supra, Thermo scientific SuperSignal).

Hippocampal Slice

Experiments were performed with 2–4-month-old male C57Bl/6 mice and 1–4-year-old naked mole-rats. Maximum life span in naked mole-rats approaches 30 years; the animals used were considered to be adult, but not senescent. Animal protocols were approved by the University of Illinois at Chicago Institutional Animal Care and Use Committee.

Transverse hippocampal slices were prepared in the conventional manner. Briefly, mice and naked mole-rats were decapitated and the brains were rapidly removed into ice-cold artificial cerebrospinal fluid (ACSF) containing (in mM): NaCl, 124; KCl, 3; KH2PO4, 1.2; NaHCO3, 26; MgSO4, 2.5; CaCl2, 3.4; Na-ascorbate, 2; and D-glucose, 10, gassed with 95% O2 and 5% CO2. The tissue was then sliced at 400 μm on a tissue chopper. Slices were placed in an interface chamber and constantly perfused (1.0 ml/min) with ACSF at 34-35C degrees for 1 hour. One mouse and one naked mole-rat were used on each day and slices from each were maintained in parallel in the same chamber for experiments. Stimulation electrodes were placed in the stratum radiatum of subfield CA1c to activate Schaffer-commissural fibers. Population recordings of synaptic field potentials (excitatory postsynaptic potentials or EPSPs) were made with micropipettes positioned in the stratum radiatum of CA1b. Evoked responses were digitized and analyzed online using custom software. Field EPSPs (fEPSPs) were evoked alternately in the mouse and naked mole-rats slices at 10 s intervals throughout experiments. Baseline stimulus intensity was set to evoke a half-maximal fEPSP in each slice. Baseline recordings were taken for at least 10 min before manipulations. Initial slope and peak

amplitude were calculated for each fEPSP and normalized to the baseline average in each slice. For anoxic depolarization experiments, O2 to the recording chamber atmosphere and perfusion ACSF was replaced with N_2. For the fructose experiments, a stable baseline was established then the perfusion solution was switched from the standard ACSF to an identical ACSF that replaced 10mM D-glucose with 10mM D-fructose-1,6-bisphospate trisodium salt hydrate (Sigma Aldrich). After one hour the perfusion medium was switched back to standard ACSF and slices were recorded for 30 minutes to analyze recovery.

Blood glucose and tissue glycogen measurement

A drop of blood was obtained from a mouse via a tail nick and a prick to the foot in the naked mole-rat. Blood glucose was measured using an Accu-Check blood glucose meter (Roche Diagnostics). Tissue glycogen was determined with a glycogen assay kit (Cayman Chemical) according to the manufacturer's instructions.

Supplementary Figures

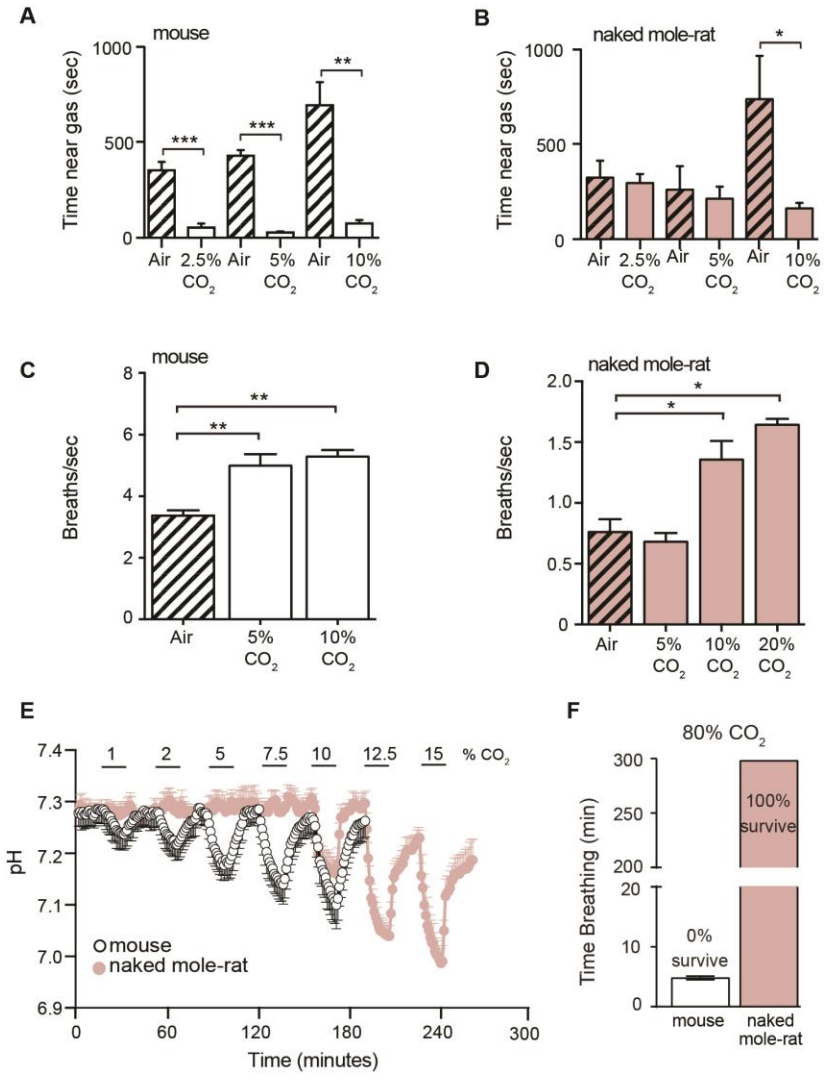

Figure S1 Reduced physiological response to hypercapnia in naked mole-rats (**A**) Mice show robust avoidance of CO_2 presented at concentrations shown. (**B**) Naked mole-rats do not avoid CO_2 gas until concentrations reach 10%. (**C**) CO_2 presented at 5 and 10% induces robust hyperventilation in mice. (**D**) Only CO_2 concentrations of 10% and above induce hyperventilation in naked mole-rats. (**E**) A pH electrode was placed in the abdomen to measure systemic extracellular pH. Inhaled CO_2 concentrations of 1% and above induce prominent tissue acidosis in mice but in naked mole-rats only CO2 concentrations above 7.5% induced acidosis. (**F**) Time breathing in 80% CO_2/20% O_2 for naked mole-rats and mice (cut-off time 300 mins). Mice did not survive any procedure whereas naked mole-rats always survived. Data shown as mean ± S.E.M. *p<0.05, **p<0.01, ***p<0.001 Student's t–test, n=4-6.

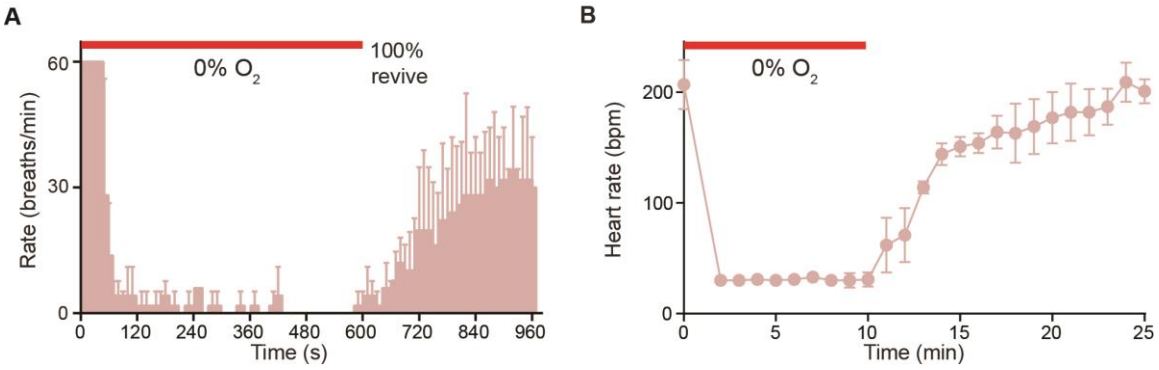

Figure S2 Anoxia resistance in naked mole-rats after a 10 minute exposure
(**A**) Respiration rate and (**B**) heart rate during 10 min of 0% O_2 showed a pattern of drastic reduction followed by recovery in the naked mole-rat. Note heart rate recovered faster after exposure to room air than in the 18 min group (Fig 1D,E).

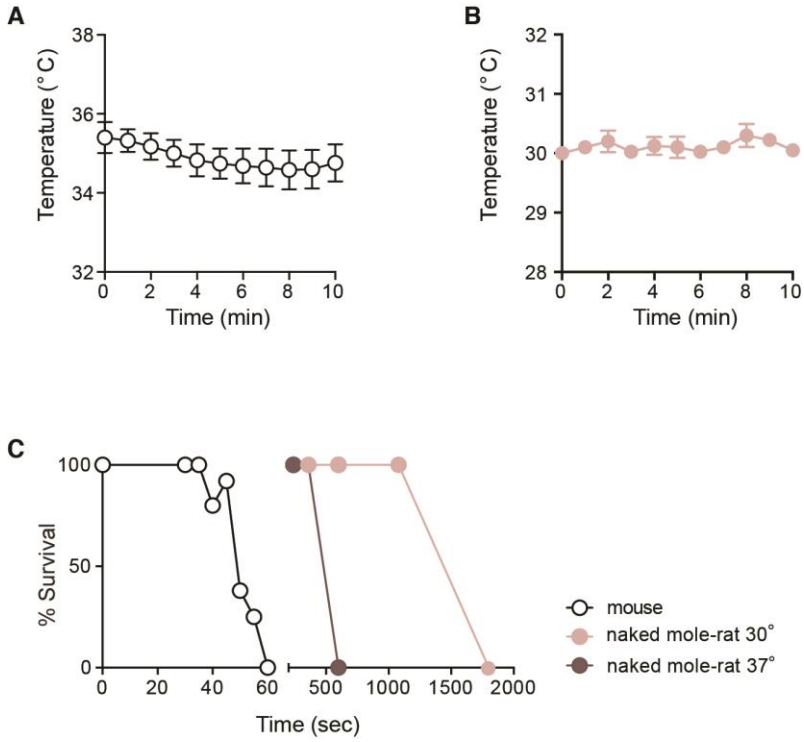

Figure S3 Temperature dependence of anoxia resistance in naked mole-rats
(A) Body temperature of mice during 10 mins of 5% O_2 exposure. (**B**) Body temperature of naked mole-rats kept at 30° during 10 mins of anoxia exposure. (**C**) Survival curves of mice and naked mole-rats maintained at 30° or 37° in 0% O_2. Naked mole-rats kept at 37° all survived 6 mins of anoxia exposure (n=3) but not 10 mins anoxia exposure compared to naked mole-rats at 30° which survived up to 18 minutes anoxia (n=3).

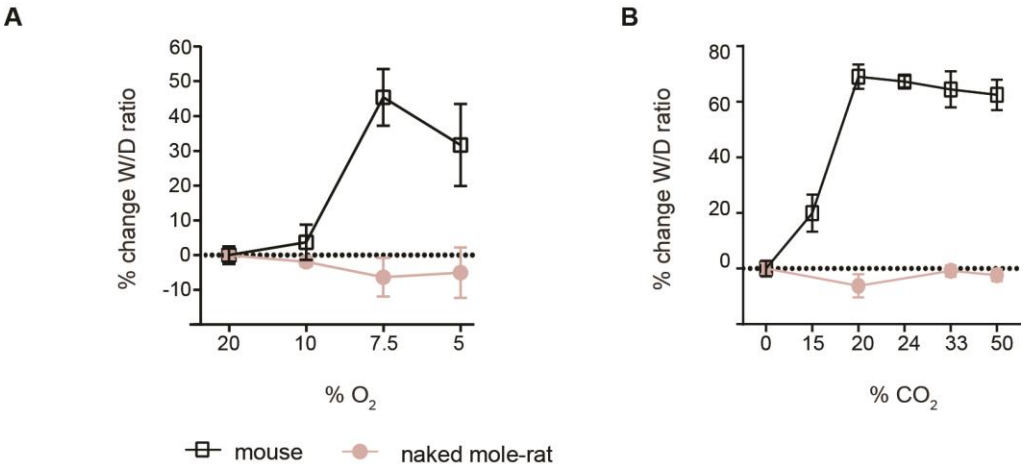

Figure S4 Pulmonary edema in mice and naked mole-rats during hypoxia and hypercapnia. The percentage change in the wet to dry weight ratio (W/D) of lung tissue was measured to assess lung edema after exposure to increasing hypoxia or hypercapnia. (**A**) Exposure to less than 10% O_2 produced severe pulmonary edema in mice but produced essentially no edema in naked mole-rats (n=3). (**B**) Concentrations of CO_2 greater than 10% also caused severe pulmonary edema in mice which was maximal above 20% CO_2. No signs of edema were observed in naked-mole-rat lung at CO_2 up to 50% (n=3).

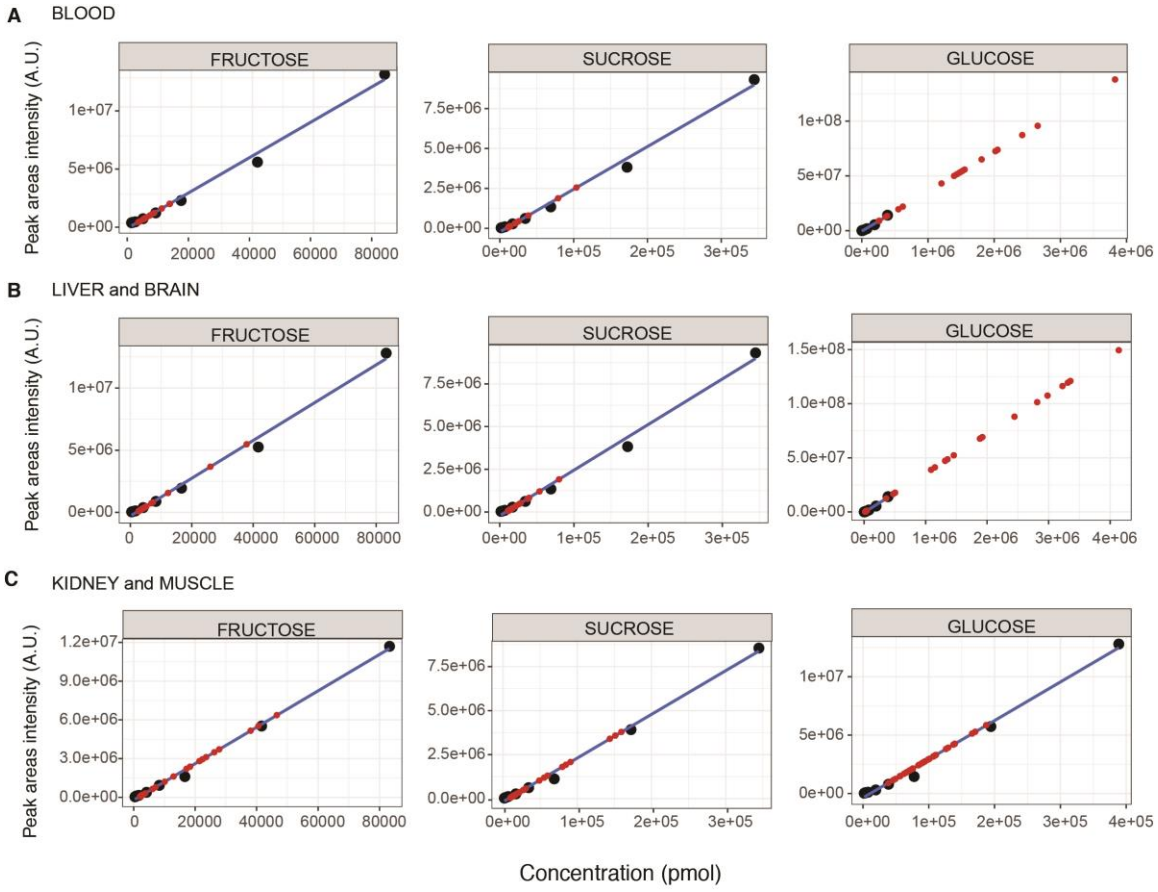

Figure S5 Calibration curves for absolute quantification of metabolites
Quantification standards (black circles) used for calibration curves to measure samples (red circles) in absolute concentrations for fructose, sucrose and glucose in (A) blood (B) liver and brain and (C) kidney and muscle. Note that glucose in blood and liver samples fell outside of the quantifiable linear part of the calibration curve in the first experiment. However, the samples were measured once more with a higher concentration of glucose standards, the absolute values for glucose (plotted in fig S8) were then recalculated from these extended calibration curves.

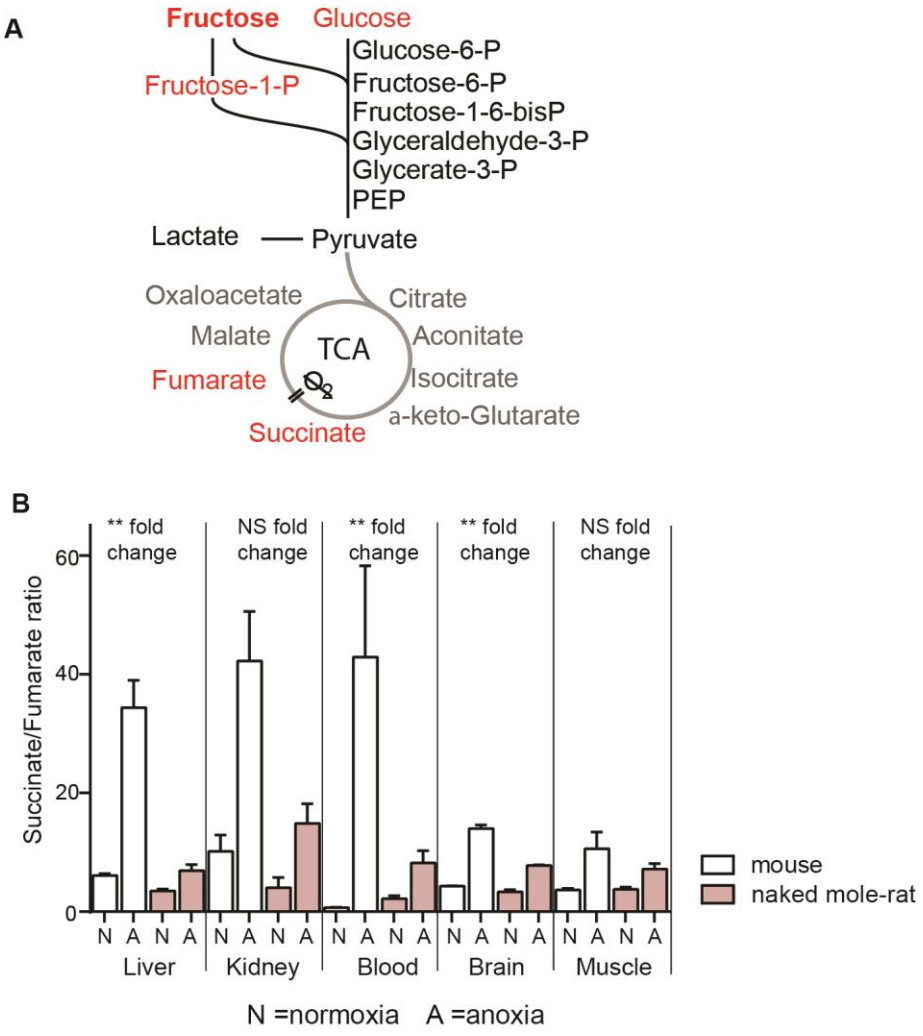

Figure S6 Suppression of mitochondrial metabolism in anoxia exposed naked mole-rats. (**A**) Schematic of glycolysis and TCA cycle where in the absence of O_2 succinate cannot be converted to fumarate. (**B**) Large increases in the succinate to fumarate ratio were observed in mouse liver, kidney blood and brain and these fold changes were significantly larger than those observed in naked mole-rat tissue after 10 min exposure to 0% O_2. Data shown as mean ± S.E.M. **p<0.01 Student's T–test, n=3.

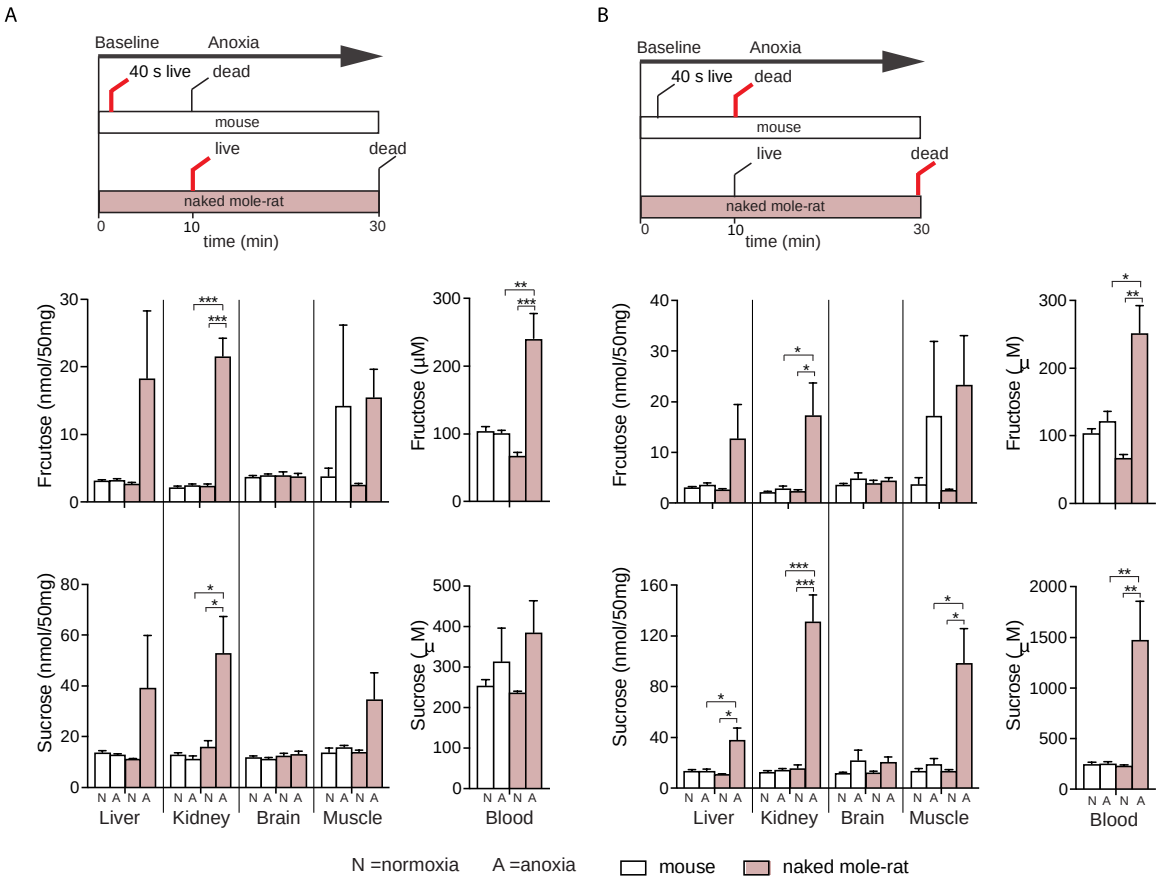

Figure S7 Increases in fructose and sucrose in tissues of naked mole-rats during exposure to anoxia. Absolute concentrations of fructose and sucrose in the liver, kidney, blood, brain and muscle of mice and naked mole-rats in normoxia compared to (**A**) 40 s anoxia for mouse and 10 mins anoxia for naked mole-rats (live:live comparison) and (**B**) 10 mins anoxia for mouse and 30 mins anoxia for naked mole-rat (dead:dead comparison). Data shown as mean ± S.E.M. *p < 0.05; **p < 0.01, ***p < 0.001 using a 2-WAY ANOVA with Bonferroni's post-hoc test, n=3.

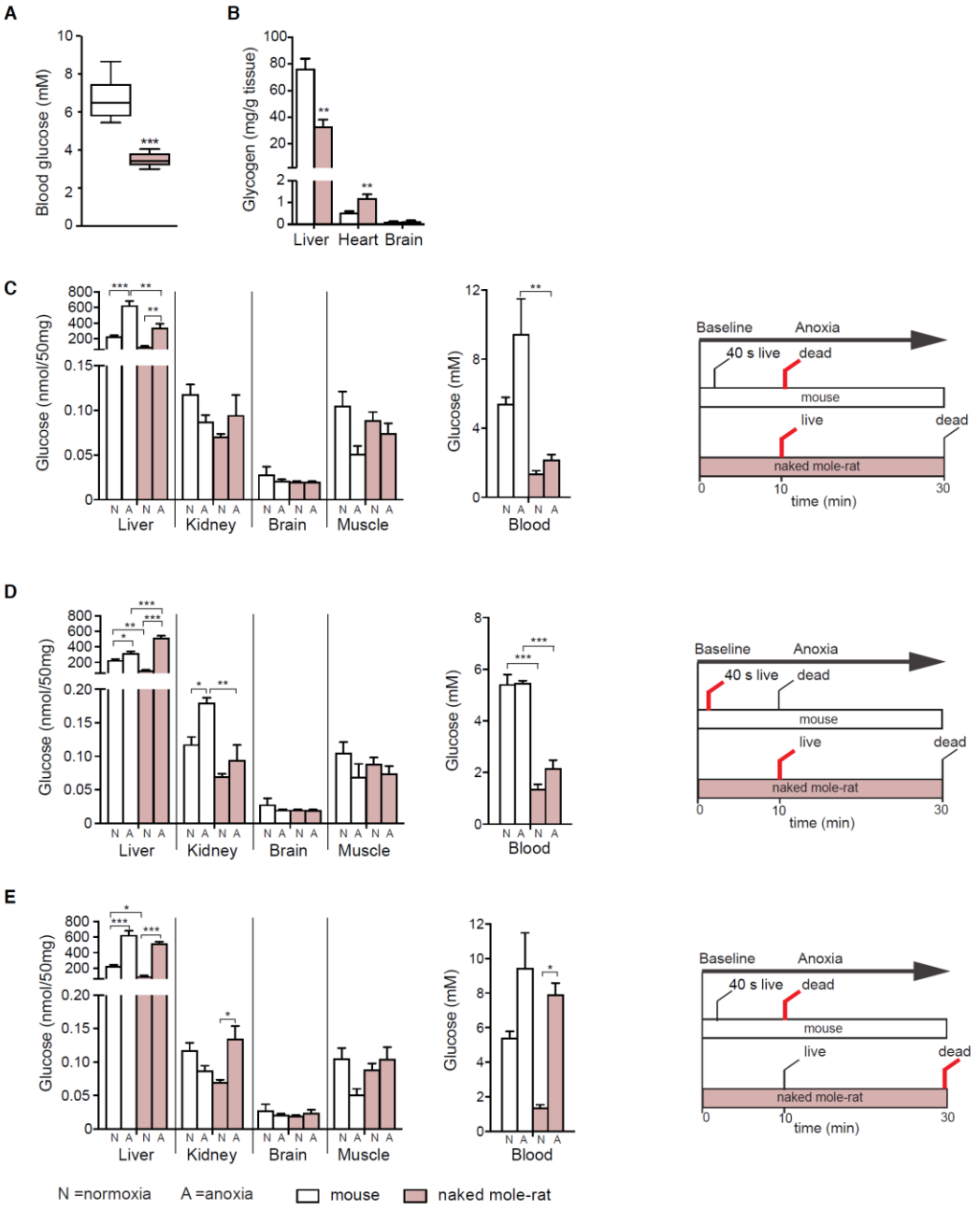

Figure S8 Glucose concentration in mouse and naked mole-rat during anoxia exposure. (A) Blood glucose concentrations in mouse versus naked mole-rat. Data shown as mean ± S.E.M. ***p<0.001 Student's t–test, n=10. **(B)** Glycogen concentrations in liver, heart and brain in mice and naked mole-rats. Data shown as mean ± S.E.M. **p<0.01 Student's t–test, n=3-6. Changes in glucose in the kidney, brain and muscle, liver and blood in mice and naked mole-rats in normoxia compared to (**C**) 10 mins anoxia for mice and naked mole-rats (**D**) 40 s anoxia for mouse and 10 mins anoxia for naked mole-rats (live:live comparison) and (**E**) 10 mins anoxia for mouse and 30 mins anoxia for naked mole-rat (dead:dead comparison). Data shown as mean ± S.E.M. *p < 0.05; **p < 0.01, ***p < 0.001 using a 2-WAY ANOVA with Bonferroni's post-hoc test, n=3.

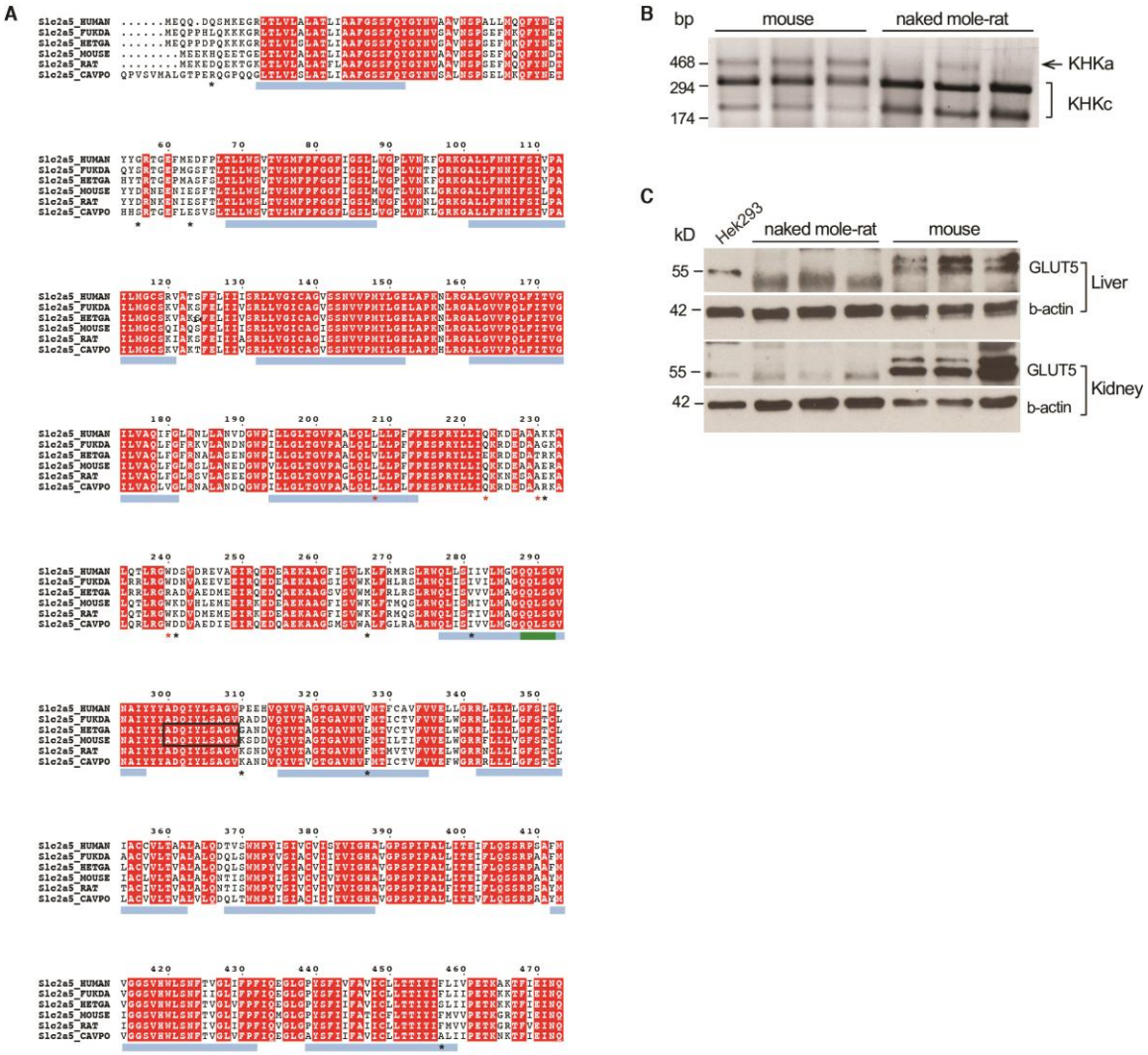

Figure S9 Multiple sequence alignment of the GLUT5 protein. (A) Alignments are shown from the guinea pig (CAVPO), mouse (MOUSE), rat (RAT), Damaraland mole rat (FUKDA), naked mole-rat (HETGA), and human proteins (HUMAN). Bars in blue indicate transmembrane domains, green bar indicates the suggested fructose binding site. Residues marked with black asterisks appear to be variants that are unique to naked mole-rats. Red asterisks indicate amino acid variants that are naked mole-rat specific but are in regions where the residue is conserved amongst the other species. Black box outlines the conserved epitope of the GLUT5 antibody **(B)** KHK-A and KHK-C isoform expression in the liver (PCR followed by HincII digestion). Upper band is the uncut KHK-A isoform, lower bands are the cut KHK-C isoform. **(C)** GLUT5 protein in Hek293 cells, naked mole-rat and mouse liver and kidney. Naked mole-rat GLUT5 protein runs slightly lower than 55kD whereas mouse GLUT5 appears as a double band. Protein content was controlled for by blotting for b-actin (n=3).

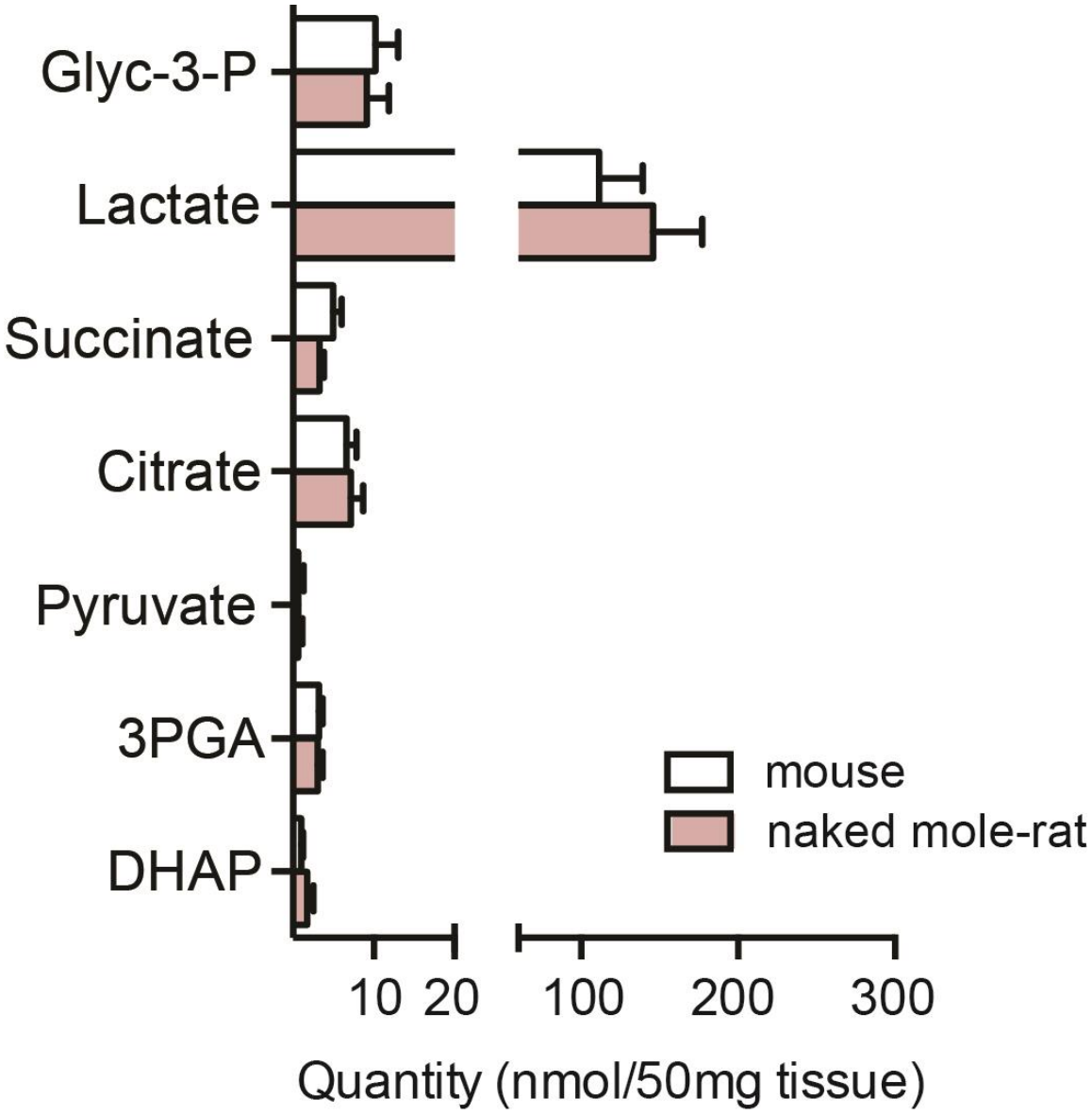

Figure S10 Absolute metabolite pools in mouse and naked mole-rat brain slices determined by GC-MS analysis. DHAP; Dihydroxyacetone phosphate, Glyceraldehyde-3-phosphate, 3-PGA; 3-Phosphoglyceric acid. (n = 12; error bars are S.E.M.)

Table S1

Comparison of heart parameters in naked mole-rat vs. mouse (Mm C57Bl/6) at 30° and 37°C

	HR	LVPsys	LVPdia	LVPdp
NMR (30°C)	196.0±13.0 *	84.7±6.2	3.8±2.2	80.9±8.3
Mm C57Bl/6 (30°C)	246.7±15.9	108.1±12.2	8.0±0.5	100.0±11.6
Mm C57Bl/6 (37°C)	400.3±53.4	93.2±4.0	7.0±2.0	86.2±2.0

Data are expressed as mean ± SEM. NMR: naked mole rat and C57/Bl6 mouse strain (measured at 30°C and 37°C); HR: heart rate in bpm, LVPsys: left ventricular systolic pressure in mmHg; LVPdia, left ventricular diastolic pressure in mmHg; LVPdp: left ventricular developed pressure in mmHg. Statistical test: one-way ANOVA with Tukey´s post-hoc test; *= $p<0.05$.

Data S1

Excel Datasheet containing mean intensity values for metabolites measured.

References and Notes

1. J. U. Jarvis, Eusociality in a mammal: Cooperative breeding in naked mole-rat colonies. *Science* **212**, 571–573 (1981). doi:10.1126/science.7209555 Medline

2. P. W. Sherman, J. U. M. Jarvis, R. D. Alexander, Eds., *The Biology of the Naked Mole-Rat* (Monographs in Behavior and Ecology, Princeton Univ. Press, 1991).

3. L.-N. Schuhmacher, Z. Husson, E. S. Smith, The naked mole-rat as an animal model in biomedical research: Current perspectives. *Open Access Anim. Physiol.* **7**, 137–148 (2015).

4. B. K. McNab, The metabolism of fossorial rodents: A study of convergence. *Ecology* **47**, 712–733 (1966). doi:10.2307/1934259

5. I. Shams, A. Avivi, E. Nevo, Oxygen and carbon dioxide fluctuations in burrows of subterranean blind mole rats indicate tolerance to hypoxic-hypercapnic stresses. *Comp. Biochem. Physiol. A* **142**, 376–382 (2005). doi:10.1016/j.cbpa.2005.09.003 Medline

6. H. Burda, R. Šumbera, S. Begall, "Microclimate in burrows of subterranean rodents – Revisited" in *Subterranean Rodents: News From Underground*, S. Begall, H. Burda, C. E. Schleich, Eds. (Springer, 2007), pp. 21–33.

7. K. M. Grimes, A. K. Reddy, M. L. Lindsey, R. Buffenstein, And the beat goes on: Maintained cardiovascular function during aging in the longest-lived rodent, the naked mole-rat. *Am. J. Physiol. Heart Circ. Physiol.* **307**, H284–H291 (2014). doi:10.1152/ajpheart.00305.2014 Medline

8. S. Lenzen, A fresh view of glycolysis and glucokinase regulation: History and current status. *J. Biol. Chem.* **289**, 12189–12194 (2014). doi:10.1074/jbc.R114.557314 Medline

9. N. C. Bennett, C. G. Faulkes, *African Mole-Rats: Ecology and Eusociality* (Cambridge Univ. Press, 2000).

10. R. Buffenstein, S. Yahav, Is the naked mole-rat *Hererocephalus glaber* an endothermic yet poikilothermic mammal? *J. Therm. Biol.* **16**, 227–232 (1991). doi:10.1016/0306-4565(91)90030-6

11. E. Blackstone, M. Morrison, M. B. Roth, H_2S induces a suspended animation-like state in mice. *Science* **308**, 518 (2005). doi:10.1126/science.1108581 Medline

12. J. F. Staples, J. C. L. Brown, Mitochondrial metabolism in hibernation and daily torpor: A review. *J. Comp. Physiol. B* **178**, 811–827 (2008). doi:10.1007/s00360-008-0282-8 Medline

13. K. B. Storey, Out cold: Biochemical regulation of mammalian hibernation – A mini-review. *Gerontology* **56**, 220–230 (2010). doi:10.1159/000228829 Medline

14. M. Pietzke, C. Zasada, S. Mudrich, S. Kempa, Decoding the dynamics of cellular metabolism and the action of 3-bromopyruvate and 2-deoxyglucose using pulsed stable isotope-resolved metabolomics. *Cancer Metab.* **2**, 9 (2014). doi:10.1186/2049-3002-2-9 Medline

15. P. H. J. L. Kuich, N. Hoffmann, S. Kempa, Maui-VIA: A user-friendly software for visual identification, alignment, correction, and quantification of gas chromatography–mass spectrometry data. *Front. Bioeng. Biotechnol.* **2**, 84 (2015). Medline

16. R. Narsai, M. Rocha, P. Geigenberger, J. Whelan, J. T. van Dongen, Comparative analysis between plant species of transcriptional and metabolic responses to hypoxia. *New Phytol.* **190**, 472–487 (2011). doi:10.1111/j.1469-8137.2010.03589.x Medline

17. V. Douard, R. P. Ferraris, Regulation of the fructose transporter GLUT5 in health and disease. *Am. J. Physiol. Endocrinol. Metab.* **295**, E227–E237 (2008). doi:10.1152/ajpendo.90245.2008 Medline

18. C. F. Burant, J. Takeda, E. Brot-Laroche, G. I. Bell, N. O. Davidson, Fructose transporter in human spermatozoa and small intestine is GLUT5. *J. Biol. Chem.* **267**, 14523–14526 (1992). Medline

19. J. Larson, T. J. T. Park, Extreme hypoxia tolerance of naked mole-rat brain. *Neuroreport* **20**, 1634–1637 (2009). doi:10.1097/WNR.0b013e32833370cf Medline

20. P. B. Garland, P. J. Randle, E. A. Newsholme, Citrate as an intermediary in the inhibition of phosphofructokinase in rat heart muscle by fatty acids, ketone bodies, pyruvate, diabetes, and starvation. *Nature* **200**, 169–170 (1963). doi:10.1038/200169a0 Medline

21. R. Buffenstein, M. Pinto, Endocrine function in naturally long-living small mammals. *Mol. Cell. Endocrinol.* **299**, 101–111 (2009). doi:10.1016/j.mce.2008.04.021 Medline

22. A. R. Manolescu, K. Witkowska, A. Kinnaird, T. Cessford, C. Cheeseman, Facilitated hexose transporters: New perspectives on form and function. *Physiology* **22**, 234–240 (2007). doi:10.1152/physiol.00011.2007 Medline

23. G. P. Dobson, E. Yamamoto, P. W. Hochachka, Phosphofructokinase control in muscle: Nature and reversal of pH-dependent ATP inhibition. *Am. J. Physiol. Regul. Integr. Comp. Physiol.* **250**, R71–R76 (1986). Medline

24. G. Mauleon, J. F. Lo, B. L. Peterson, C. P. Fall, D. T. Eddington, Enhanced loading of Fura-2/AM calcium indicator dye in adult rodent brain slices via a microfluidic oxygenator. *J. Neurosci. Methods* **216**, 110–117 (2013). doi:10.1016/j.jneumeth.2013.04.007 Medline

25. J. Hallfrisch, Metabolic effects of dietary fructose. *FASEB J.* **4**, 2652–2660 (1990). Medline

26. A. M. Port, M. R. Ruth, N. W. Istfan, Fructose consumption and cancer: Is there a connection? *Curr. Opin. Endocrinol. Diabetes Obes.* **19**, 367–374 (2012). doi:10.1097/MED.0b013e328357f0cb Medline

27. H. Liu, D. Huang, D. L. McArthur, L. G. Boros, N. Nissen, A. P. Heaney, Fructose induces transketolase flux to promote pancreatic cancer growth. *Cancer Res.* **70**, 6368–6376 (2010). doi:10.1158/0008-5472.CAN-09-4615 Medline

28. L. Tappy, K.-A. Lê, Metabolic effects of fructose and the worldwide increase in obesity. *Physiol. Rev.* **90**, 23–46 (2010). doi:10.1152/physrev.00019.2009 Medline

29. P. Mirtschink, J. Krishnan, F. Grimm, A. Sarre, M. Hörl, M. Kayikci, N. Fankhauser, Y. Christinat, C. Cortijo, O. Feehan, A. Vukolic, S. Sossalla, S. N. Stehr, J. Ule, N. Zamboni, T. Pedrazzini, W. Krek, HIF-driven SF3B1 induces KHK-C to enforce fructolysis and heart disease. *Nature* **522**, 444–449 (2015). doi:10.1038/nature14508 Medline

30. V. Chu, J. M. Otero, O. Lopez, J. P. Morgan, I. Amende, T. G. Hampton, Method for non-invasively recording electrocardiograms in conscious mice. *BMC Physiol.* **1**, 6 (2001). doi:10.1186/1472-6793-1-6 Medline

31. UniProt Consortium, UniProt: A hub for protein information. *Nucleic Acids Res.* **43**, D204–D212 (2015). doi:10.1093/nar/gku989 Medline

32. K. D. Pruitt, G. R. Brown, S. M. Hiatt, F. Thibaud-Nissen, A. Astashyn, O. Ermolaeva, C. M. Farrell, J. Hart, M. J. Landrum, K. M. McGarvey, M. R. Murphy, N. A. O'Leary, S. Pujar, B. Rajput, S. H. Rangwala, L. D. Riddick, A. Shkeda, H. Sun, P. Tamez, R. E. Tully, C. Wallin, D. Webb, J. Weber, W. Wu, M. DiCuccio, P. Kitts, D. R. Maglott, T. D. Murphy, J. M. Ostell, RefSeq: An update on mammalian reference sequences. *Nucleic Acids Res.* **42**, D756–D763 (2014). doi:10.1093/nar/gkt1114 Medline

33. R. C. Edgar, MUSCLE: Multiple sequence alignment with high accuracy and high throughput. *Nucleic Acids Res.* **32**, 1792–1797 (2004). doi:10.1093/nar/gkh340 Medline